

# Role of imidazole edge to edge supramolecular interaction in the crystal packing of Cu(II)(SCN<sup>-</sup>)<sub>2</sub>(imidazole)<sub>2</sub> complex: A novel variety of supramolecular interaction revealed by CCDC database analysis and explored through DFT computational studies



Sirajuddin Sarkar<sup>a</sup>, Sourav Ranjan Ghosh<sup>a,b</sup>, Paula Brandão<sup>c</sup>, Atish Dipankar Jana<sup>a,\*</sup>

<sup>a</sup> Department of Physics, Behala College, Parnasree, Kolkata – 700092, West Bengal, India

<sup>b</sup> Department of Physics, Heritage Institute of Technology, Anandapur, Kolkata-700107, West Bengal, India,

<sup>c</sup> Departamento de Química, Universidade de Aveiro, 3810-193 Aveiro, Portugal

## ARTICLE INFO

### Article history:

Received 26 October 2019

Revised 20 October 2020

Accepted 22 October 2020

Available online 23 October 2020

### Keywords:

Imidazole edge to edge supramolecular interaction

DFT

RDG

NCI

Hydrogen bonding

## ABSTRACT

Crystalline molecular solids are self-assembled entities in which molecular components are packed by various intermolecular forces. A novel edge to edge supramolecular interaction between the imidazole molecules has been observed in the crystal packing of the coordination complexes Cu(II)(SCN<sup>-</sup>)<sub>2</sub>(imidazole)<sub>2</sub>. In this edge to edge interaction, one of the C-N bonds of an imidazole molecule exhibit non-bonded interaction with the complementary C-N bond of another imidazole molecule with no facial overlap between the imidazole molecules. This edge-to-edge interaction of imidazole molecules along with NH...S, CH...S interaction governs the packing of molecular complexes in the solid state. Basis set superposition error corrected interaction energy of this edge to edge supramolecular interaction of imidazole has been estimated to be -2.59 kcal/mole. The electronic nature of this novel intermolecular interaction has been computed through DFT methodology. A CCDC database search has revealed that, a sizable number of crystals containing imidazole moiety shows this type of edge to edge supramolecular interaction. Hirshfeld surface analysis shows that this edge to edge interaction play cooperative role along with other intermolecular forces in the crystal packing of the present complex.

© 2020 Elsevier B.V. All rights reserved.

## 1. Introduction

Weak intermolecular forces, especially hydrogen bonding [1] and others [2–4] have drawn the attention of the scientific community in their pursuit of designing functional molecular materials [5]. Proper understanding of these weak intermolecular forces is still a great challenge, as a slight variation in the molecular skeleton leads to quite different self-assembled molecular motifs. Though, currently we are entering into an era of dynamic self-assembly [6], crystalline materials which represent equilibrium self-assembled structures, still continue to guide us regarding many subtle features of molecular self-assembly, especially about the nature of intermolecular forces itself. A judicious use of various weak forces have enabled scientists to design and realize various types of functional materials among which reversible [7] and

adaptive [8] stimuli responsive systems are one of the hot topics in the current scientific literature related to functional materials.

In the present paper we report a novel type of weak supramolecular force between imidazole molecules where two imidazole molecules interact with each other at one of their edges only. In the crystal structure of a three-component coordination complex involving Cu, imidazole and thiocyanate, we see that edge to edge C-N...C-N... cyclic supramolecular synthon is present between two imidazole molecules which has played a subtle role in crystal packing. This edge to edge interaction of imidazole molecules along with other weak hydrogen bonding forces like NH...S, CH...S and van der Waals interactions have governed the molecular packing in the present crystal. The main focus of the present paper is to highlight the energetic and electronic nature of this novel edge to edge supramolecular interaction between imidazole molecules. Towards this, we have carried out DFT computational studies to assess the binding energy of this edge to edge interaction along with other modern tools like non-covalent interaction (NCI [9,10]) analysis, reduced density gradient (RDG [11,12]) analysis and atoms in molecule (AIM [13]) analysis. The nature of

\* Corresponding author.

E-mail address: [atishdipankarjana@yahoo.in](mailto:atishdipankarjana@yahoo.in) (A.D. Jana).

electron delocalization has been studied through the nucleus independent chemical shift (NICS) [14,15] analysis. Crystal, which is a “supermolecule par excellence” [16], is packed due to the intriguing competition as well as cooperation of multiple weak forces, each having some contribution. Hirshfeld surface analysis [17], which is based on the experimental electron density, is a versatile tool to unravel the relative importance of various weak forces in the molecular packing. We have employed Hirshfeld surface analysis to explore the role of edge to edge interaction between imidazole molecules along with other weak forces operating in the crystal. A Cambridge Structural Database (CSD) analysis has also been carried out to explore the propensity of this type of edge to edge supramolecular interaction between imidazole molecules in imidazole containing molecular crystals. This has revealed that the edge to edge supramolecular interaction between imidazole molecules is not a mere chance occurrence in the present crystal, but it is rather present in a sizable number of imidazole bearing molecular crystals in the CSD database. To the best of our knowledge, though this type of edge to edge interaction between imidazole molecules has been found to be present in many crystals in the CSD database, yet, this novel supramolecular interaction was not highlighted in any previous report. In the present paper we have explored this interaction through a varieties of modern computational tools and conclude that imidazole edge to edge supramolecular interaction is another weak force which can influence crystal packing in favorable situations.

## 2. Materials and methods

All solvents and reagents were obtained commercially and used without further purification.

### 2.1. Synthesis of Cu(II)(SCN<sup>-</sup>)<sub>2</sub>(imidazole)<sub>2</sub>

136 mg (2mmol) of imidazole was dissolved in 10ml distilled water and then it was added dropwise to a previously prepared (181mg, 1mmol) copper acetate solution (in 20ml water). The colourless solution turns deep blue. To this deep blue coloured reaction mixture 10ml aqueous solution of 152mg (2mmol) ammonium thiocyanate was added which quickly turned the deep blue colour of reaction mixture into light blue colour. The light blue coloured solution was then kept inside a thermostat at 15°C for crystallization. Greenish block-shaped single crystals of Cu(II)(SCN)<sub>2</sub>(C<sub>3</sub>H<sub>4</sub>N<sub>2</sub>)<sub>2</sub> were obtained within 24 hours.

### 2.2. X-ray crystallography

X-ray diffraction data for the crystalline compound was collected at 150K on a diffractometer equipped with Bruker Kappa Apex-II CCD area-detector using MoK<sub>α</sub> ( $\lambda=0.71073 \text{ \AA}$ ) radiation. The structure was solved by direct method using SHELXS-2017 and refined with a full-matrix least-squares technique employing the SHELXL-2017 program package [18]. Anisotropic thermal parameters were applied to all the non-hydrogen atoms. Imidazole – NH hydrogen atoms were located from the difference Fouriermap whereas all other hydrogen atoms were fixed to their respective parent atoms according to the atom riding model. Crystallographic information for **1** has been deposited to the Cambridge Crystallographic Data Center (CCDC) which bears the CCDC No. 1884050. Crystal data, as well as details of data collection and refinement for the complex, has been summarized in Table S1. Selected bond distances and bond angles are listed in Table S2, and hydrogen bond parameters have been presented in Table 1.

## 2.3. Theoretical Calculations

The optimized geometry and the electronic structure of two imidazole units have been explored the DFT computation. Geometry optimization has been performed using the Gaussian-03 package. [19] Initial geometry of the edge to edge interacting supramolecular dimeric motif of two imidazole molecules was adopted from the crystal structure. 6-311g(d,p) basis set and B3LYP hybrid density functional was used for geometry optimization. The binding energy (B.E.) of the edge-to-edge interacting supramolecular system of two imidazole molecules has been estimated according to the formula, B.E.= (Energy of the motif) - 2\*(Energy of a single molecule). Basis set superposition error (BSSE) correction was incorporated using Counterpoise correction scheme. Besides geometry optimization, the nature of variation of intermolecular interaction potential has also been studied for the sidewise horizontal shift of one of the imidazole molecules with respect to the other. This computation has been carried out using M06-2X functional using the pgi-Linux-2018 version of the GAMESS [20] to take into account the dispersion interaction. Non-covalent interaction (NCI), reduced density gradient, and AIM analysis have been carried out using the Multiwfn 3.6 package [21]. NICS study has been carried out using the Gaussian-03 package for the dimeric motif optimized at 6-311g(d,p) level. BSSE corrected binding energy for hydrogen bonded imidazole ... thiocyanate supramolecular system was computed at the same level of theory as that of the imidazole edge to edge interaction using Gaussian-03 package.

### 2.4. Hirshfeld surface analysis

A deeper insight into the molecular packing forces can be gained by Hirshfeld fingerprint and surface analysis. Hirshfeld fingerprint plot is a 2D visualization methodology for intermolecular interactions and Hirshfeld surface plot is a 3D visualization tool. 2D fingerprint plots contain distinct spikes each characterizing a particular intermolecular interaction. In Hirshfeld surface plot, red colour-coded regions around the molecules denote points of closer intermolecular contacts. These plots provide relative importance of various weak intermolecular forces responsible for a particular pattern of molecular self-assembly in a given crystal structure. 3D Hirshfeld surface plots are generated in terms of the parameter  $d_{\text{norm}}$  called normalized contact distance.  $d_{\text{norm}}$ , on the other hand, is related with two parameters  $d_e$  (the distance from the point to the nearest atoms external to the surface) and  $d_i$  (the distance to the nearest atoms internal to the surface) and the van der Waals (vdW) radii of the each atom according to Eq. (1).

$$d_{\text{norm}} = \frac{d_i - r_i^{\text{vdW}}}{r_i^{\text{vdW}}} + \frac{d_e - r_e^{\text{vdW}}}{r_e^{\text{vdW}}} \quad (1)$$

A negative  $d_{\text{norm}}$  value (deep red regions on the surface plot) indicate shorter intermolecular contacts than the vdW contact. On the other hand, a positive (deep blue regions on the surface plot) value of  $d_{\text{norm}}$  indicates intermolecular contacts which are longer than vdW contact. Regions depicted in white colour correspond to contact distances that are around the vdW separation. The distribution of the  $d_{\text{norm}}$  values in 3D space around the molecule or molecular system convey how important a particular region of the molecule is for intermolecular interactions. CrystalExplorer 3.1 program [22] has been used to analyse X-ray structural electron density distribution to generate fingerprint and surface plots.

### 2.5. CCDC database analysis

To assess the statistical significance of the newly noticed edge to edge supramolecular interaction between imidazole molecules, a Cambridge Structural Database (CSD June 2018 release) search has

**Table 1**  
Hydrogen Bond table ( $\text{\AA}$ ,  $^\circ$ )

D-H...A	D-H( $\text{\AA}$ )	H...A( $\text{\AA}$ )	D...A( $\text{\AA}$ )	$\angle$ D-H...A( $^\circ$ )	Symmetry
N2-H2A..S	0.80	2.58	3.3769(17)	170	-x,-y,1-z
C1-H1...N3	0.95	2.49	2.929(2)	108	Intramolecular

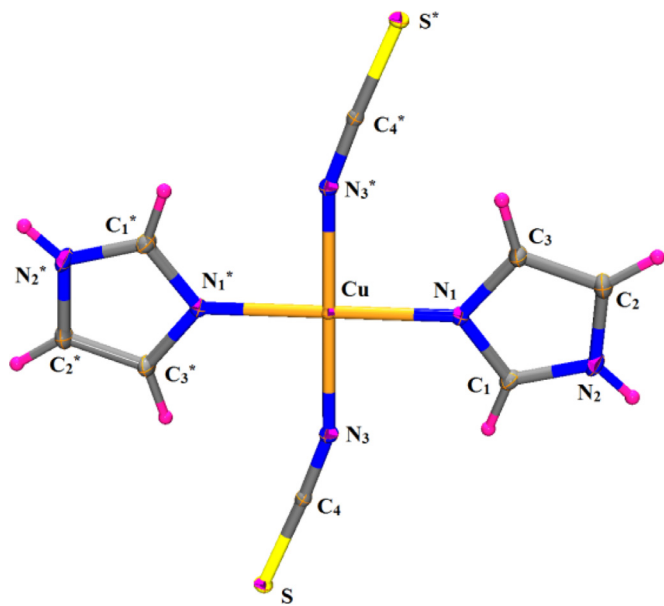


**Fig. 1.** The ORTEP diagram of the complex (30% ellipsoidal probability) with atom numbering scheme (\* = -x, -y, -z).

been carried out. With the help of ConQuest 1.23 module of CSD, a search criterion for intermolecular edge to edge close contact was set, where C...N and N...C distances were restrained between 2.5 $\text{\AA}$  to 4.5 $\text{\AA}$ , R-factor was less than 0.1 and no-disorder structures were considered. In total, 163 hits were generated (Table S3) which contains both organic as well as metal-organic compounds. It was observed that most of the structures were metal-organic compounds though some were organic only systems containing imidazole and its substituents. Each of the structures was manually checked for the imidazole edge-edge interaction. The results of this analysis have been presented in section 3.1.4.

### 3. Results and discussion

#### 3.1. X-ray crystal structure

##### 3.1.1. Description of the coordination complex

X-ray structural analysis reveals that the crystalline solid consists of square-planar mononuclear  $\text{Cu}(\text{II})(\text{SCN}^-)_2(\text{imidazole})_2$  units. The ORTEP diagram of the complex has been depicted in Fig. 1.  $\text{Cu}(\text{II})$  ion occupies the centre of inversion. The asymmetric unit consists of  $\text{Cu}(\text{II})$  ion along with one  $\text{SCN}^-$  anion and one imidazole ligand.  $\text{Cu}(\text{II})$  has square planar coordination geometry with four N atoms (two contributed by two  $\text{SCN}^-$  and other two contributed by two imidazole ligands) occupying the four coordination sites.  $\text{Cu-N1(imidazole)}$  bond distance is 2.0127(13) $\text{\AA}$  and  $\text{Cu-N3(thiocyanate)}$  bond distance is 1.9688(12) $\text{\AA}$ . The bond angle between N1-Cu-N3\* is 90.29(5) $^\circ$  and the bond angle between N1-Cu-N1\* is 89.71(5) $^\circ$ . The bond angle between N1-Cu-N1\* is 180 $^\circ$  and the bond angle between N3-Cu-N3\* is 180 $^\circ$ . Here the thiocyanate S-C4-N3 bond is deviated by an angle is 176.96(15) $^\circ$ . The bond angle between Cu-N1-C1 is 125.5(10) $^\circ$  and Cu-N1-C1 is 129.57(16) $^\circ$ .

#### 3.1.2. Supramolecular Assembly

Molecular complexes have self-assembled into a layered structure in the crystal (Fig. 2). Three such layers pass through a unit cell. These layers are (001) crystallographic planes. Within a layer, molecular units are relatively strongly bound by hydrogen bond, edge to edge C-N...N-C interaction between imidazole molecules, Cu...S interaction compared to the interlayer interaction is weaker van der Waals nature. The packing pattern of the molecular layers within the crystal is a Herring-bone type which is a commonly observed molecular packing motif [23]. Individual supramolecular layers constitute the (001) plane of the crystal (Fig. 3a). Within a layer molecular complexes are assembled into a tape-like supramolecular architecture (Fig. 3b) through cooperative weak  $\text{CH}\cdots\text{S}$  (2.929(2)) and strong  $\text{NH}\cdots\text{S}$  (3.3769(17)) hydrogen bonds. These supramolecular tapes run along [110] direction. Adjacent tapes are joined at both edges by the edge to edge C-N...N-C interaction leading to the layered assembly. Within a tape, terminal S atoms of coordinated thiocyanate act as a common acceptor for -NH group of coordinated imidazole and a -CH unit of the same imidazole opposite to the -NH group. Geometrical parameters for these hydrogen-bonding interactions have been given in Table 1. Successive tapes run diagonally along [110] direction and interact with each other through C-N...N-C interaction where imidazole moiety of one unit belonging to a particular tape interact with another imidazole moiety located on the adjacent tape. This novel mode of C-N...N-C supramolecular interaction has been further depicted in Fig. 4. The imidazole molecules from adjacent tapes interact at their edges opposite to the coordinated N atoms. The mode of this interaction is quite different from conventional cycle stacking interaction. Whereas the conventional stacking interaction of benzene molecules are face to face or edge to edge [24], the interaction among the imidazole molecules in the present crystal structure is an edge to edge one without any degree of facial overlapping. This supramolecular interaction is between the N-C edges of two interacting imidazole molecules [Fig. 4] where C...N and N...C supramolecular contacts are observed. The distance between N and C atom is 3.303(2) $\text{\AA}$ . A Cu...S interaction is also responsible for the layered supramolecular assembly. S atoms contributed by thiocyanate coordinatively interact along the axial direction of the Cu ions. The Cu...S distance is 3.069(5) $\text{\AA}$ .

#### 3.1.3. DFT optimized structure of edge to edge interacting dimeric motif of imidazole

It is interesting to note that the edge to edge supramolecular interaction among imidazole molecules in the present crystal structure is such that the closest contact between the pair of interacting molecules is only between two edges of the pair of interacting molecules. The edge to edge interaction between two imidazole units seen in the present crystal structure appears intriguing at a first look. To verify the feasibility of possible edge to edge supramolecular interaction between imidazole molecules a geometry optimization was attempted with the crystal geometry of the interacting motifs as input. The computed optimized geometry of the edge to edge interacting pair of imidazole molecules was found to be very close to that found in the crystal structure.

One of the important supramolecular motifs observed in the crystal structure is the edge to edge interacting motif of two imidazole molecules (Fig. 4(I) left panel). To explore the electronic nature of this interaction, we have optimized the geometry of

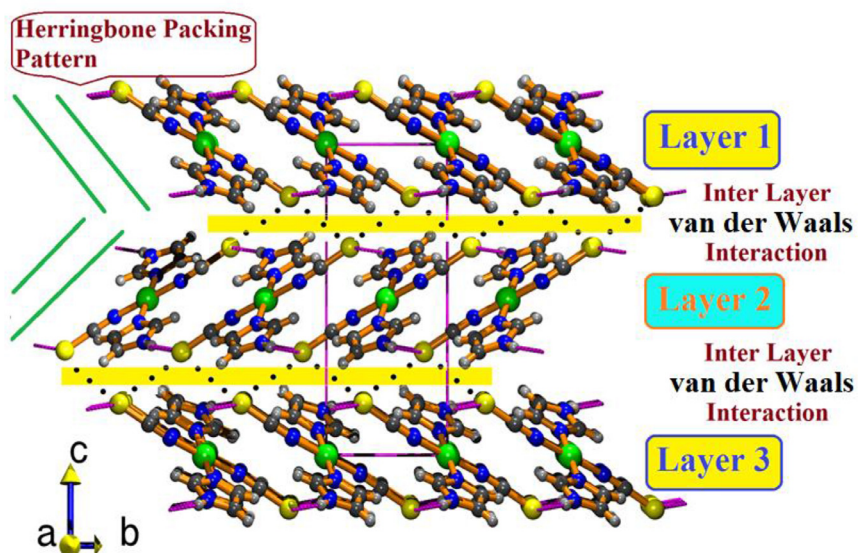


**Fig. 2.** Three dimensional packing of molecular complexes in the layer form.

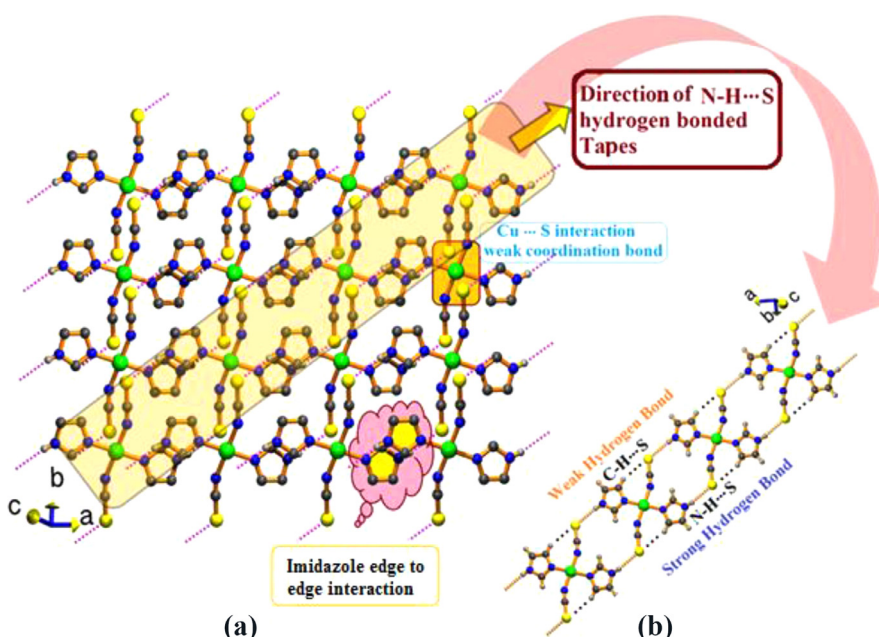


**Fig. 3.** (a). 2D supramolecular layer (001) of the molecular complexes assembled through N-H...S and imidazole edge to edge supramolecular interaction (b) Supramolecular tapes formed by cooperative weak (C-H...S) and strong (N-H...S) hydrogen bonds.

this supramolecular motif. The optimized geometry comes out to be very close to that found in the crystal structure (Fig. 4(I) right panel). The supramolecular motif of two interacting imidazole molecules has formed through edge to edge interaction where one of the C-N edge of a imidazole molecule interacts with the complementary N-C edge of the another imidazole molecule. This supramolecular interaction brings C and N atoms on the complementary edges closer together producing a cyclic synthon (C-N...C-N...). The distance between the interacting carbon and nitrogen atoms on the complementary edges is 3.285 Å (DFT) and 3.303(2) Å (Crystal). The basis set superposition error (BSSE) corrected interaction energy of this edge to edge interacting supramolecular motif has been found to be -2.59 kcal/mole. Fig. 4(II)(a) depicts the electrostatic potential map of two interacting imidazole molecules. It can be observed that the interacting C-N edges are slightly polarized which is expected due to the electronegativity differences be-

tween C and N atoms. This polarized nature of the CN bond should be contributing to the edge to edge supramolecular interaction between imidazole molecules. Fig. 4(II)(b) to 4(II)(h) depicts some of the delocalized orbitals for the interacting molecules. Both HOMO, LUMO, HOMO-1 and HOMO-5 show substantial delocalization. This delocalized electron clouds can be assumed to be involved in the edge to edge supramolecular interactions between the imidazole molecules.

Besides geometry optimization, another way to explore the authenticity of this edge to edge interaction was also attempted in which it was expected that a potential minima at this configuration should be observed when one of the molecules of the interacting pair is shifted horizontally leading to varying degree of overlapping area between the faces of the two interacting molecules. One of the two imidazole molecules (fragment-II) was thus shifted horizontally (x-direction) keeping its vertical separation (z-height)

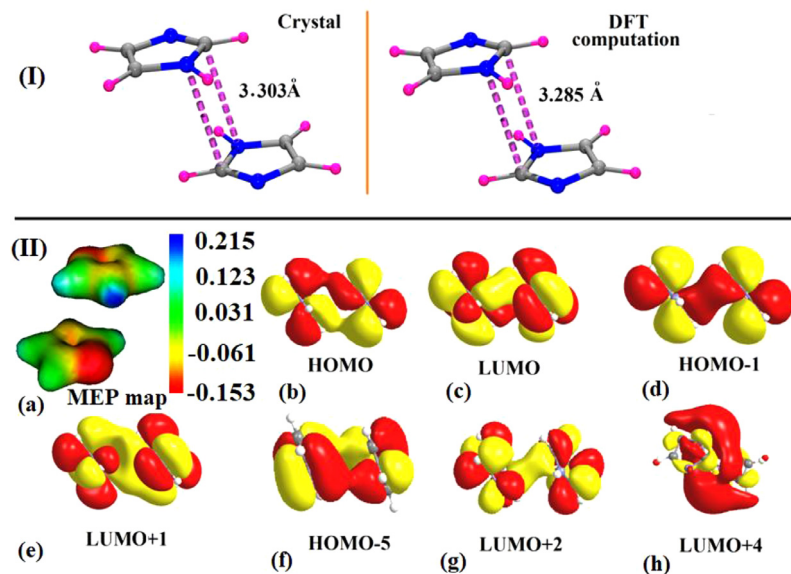


**Fig. 4.** (I). Crystal geometry and corresponding DFT optimized geometry of edge to edge interacting supramolecular motif of two imidazole molecules, (II) (a) Molecular electrostatic potential (MEP) map, (b) HOMO (c) LUMO (d) HOMO-1 (e) LUMO+1 (f) HOMO-5 (g) LUMO+2 (h) LUMO+4 of edge interacting imidazole molecules.

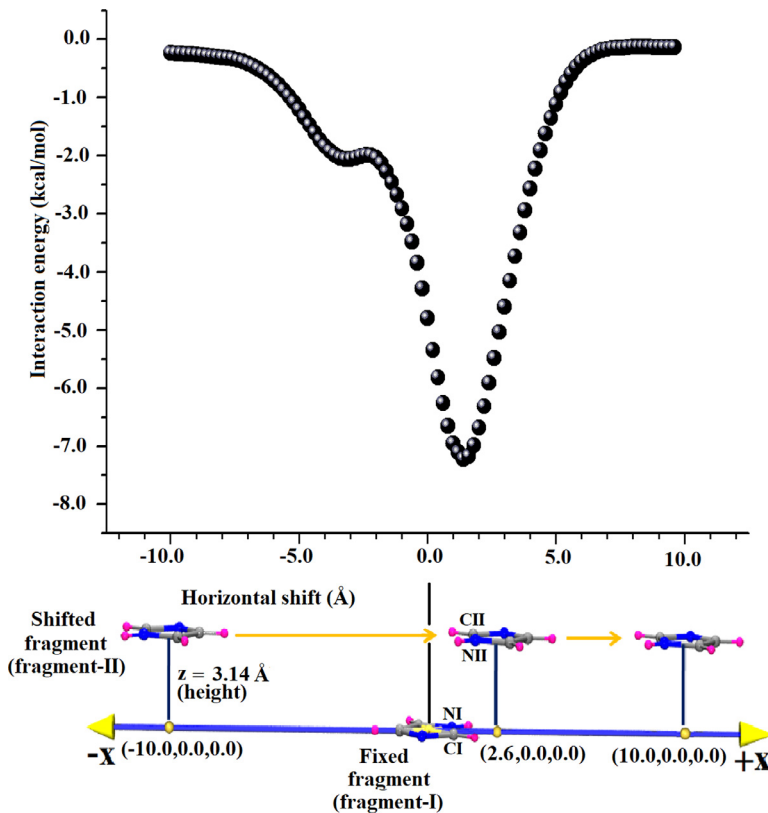


**Fig. 5.** The variation of interaction potential between two stacked imidazole molecules when one of them is translated horizontally over the other causing varying degree of face to face overlap. The deep in the potential energy curve occurs in the edge to edge configuration with least face to face overlap.

fixed at 3.14 Å (the height in crystal) with respect to the other molecule (fragment-I), whose centroid was chosen as the origin (Fig. 5). Fragment-II was initially placed far left to the origin at a distance  $x = -10$  Å and its  $x$  coordinate was gradually incremented by 0.2 Å in each step to bring it to a point  $x = +10$  Å which is far right to the origin. The molecules were aligned in such a way that  $x$ -axis passes through the centroid of fragment-I and the middle of the CI-NI bond edge. In this configuration interacting C-N edges

(CI-NI and CII-NII) of the two fragments were parallel to each other and are aligned parallel to Y-axis. At each 0.2 Å step the interaction potential was computed using M06-2X density functional and 6-311G(d,p) basis set. The variation of the interaction energy has been depicted in Fig. 5, which clearly shows a deep in the interaction potential curve at a horizontal separation of +1.6 Å. This deep in the potential curve can be assigned to the optimal edge to edge supramolecular interaction between two imidazole units as

we argue here. The distance between centroid I corresponding to fragment-I and the projection point of centroid II of fragment-II in the ring plane of fragment-I in our crystal is 2.64 Å. The deep of the potential curve is occurring not at x=0.0 Å (would have corresponded to face to face cycle stacking interaction) but at +1.6 Å, which is approximately at the middle of the separation between the x-coordinates (0.0 Å and 2.64 Å) of the centroids of the two fragments. At this conformation the CII-NII edge of fragment II has just passed over to the right of the NI-Cl edge of fragment-I. At this configuration there is no face to face overlap of the two fragments but the interaction is mostly between the NI-Cl and CII-NII complementary edges. The orbital analysis of the optimized geometry described in the previous section also corroborates this argument. Thus the edge to edge supramolecular interaction between imidazole molecules (eeimi) appears to be authentic in nature and its existence in a particular crystal may not be doubted as a crystal packing effect. To further verify the authenticity of this interaction we have searched for possible occurrences of this type of edge to edge interaction between imidazole units in other imidazole containing molecular crystals present in the Cambridge structural database (CSD), the result of which has been presented in the next section.

#### 3.1.4. CSD database analysis of edge-to-edge supramolecular interaction of imidazole

The analysis of the edge to edge supramolecular interaction between a pair of imidazole molecules in the crystal structures retrieved from the CSD database have been carried out based on following five geometrical parameters: (i) C-N distances (CI...NII and NI...CII), where CI-NI and CII-NII are respective edges of interacting fragment-I and fragment-II; (ii) the angle Cg1-Cl-NII, where Cg1 is the centroid of imidazole fragment-I; (iii) Perpendicular distance of the projection of Cg1 onto the ring plane of fragment-II (Cg1-M), where M is the middle point of CII-NII edge of fragment-II; (iv) The distance between Cl and NII(Cl-NII), where NII is the point of projection of the NII atom on the ring plane of fragment-I; (v) The distance between Cg1 and Cg2; where Cg2 is the projection of the centroid of fragment-II (Cg2) onto the ring plane of fragment-I. An understanding of the geometries of these parameters can be easily obtained from the Fig-6(a). The results of these analysis have been presented as five histogram plots Fig. 6(b) to (f). Fig. 6(b) shows the histogram plot of the distribution of C...N distances with the number of structures. It can be seen that the peak in this distribution appears around 3.5 Å. The distribution has a broad peak, most of the structures (74.5%) fall within four beans centred in the range 3.2 to 3.8 Å. The histogram plot of the distribution of Cg1-Cl-NII angle has been depicted in Fig 6(c) which shows that this histogram plot peaks around 75° and tails off till 120°. No structure was retrieved for which this angle is less than 60°. There is a deep around 90° to 100° range in this histogram plot, and then another small peak occurs in the 100° to 120° range. For values of this angle greater than 90° there will be no facial overlap between two molecules. A structure by structure manual verification of the retrieved structures has revealed that when this angle become less than ~70° then only more than 50% overlap in the area of two rings occur, in which case it is more likely to be face cycle stacking interaction. For the value of this angle greater than 75° there is less than 25% facial overlap and the interaction can be treated as an edge to edge one.

The centroid to projected centroid distance (Cg1-Cg2) is also another measure of the degree of facial overlap between the two interacting imidazole rings. The distance between CN edge and the opposite carbon atom of an imidazole unit is approximately 2.28 Å. When Cg1-Cg2 distance is greater than 2.28 Å then there is no facial overlap at all and when this distance is around 0.0 Å then there is around 100% facial overlap of the interacting rings. The fre-

quency of structures in different Cg1-Cg2 distance range has been depicted in Fig. 6(f) which reveals that for most of the structures this distance is in the range 1 Å to 2 Å. There are a very few structures for which this distance is less than 1 Å for which true face to face cycle stacking interaction occurs. At 0.75 Å Cg2 will just touch the edge of fragment-I, and facial overlap will be around 50%. So, Fig. 6(f) reveals that for the lion's share of structures the facial overlap is much less than 50% in which case the interaction is mostly edge-to-edge in nature.

The frequency distribution with respect to Cg1-M distance shown in Fig. 6(d) also correlates well with the assertion that most favourable supramolecular stacking interaction for imidazole molecules is the edge-to-edge one instead of being a face to face interaction. For a genuine face to face interaction this distance should become negative in which case Cg1 will be within the periphery of ring II. For complete face to face overlap Cg1-M distance should be -1.14 Å which is the centroid to CN-edge distance of an imidazole ring. Data from Fig 6(d) reveals that for most of the structures this distance fall in the range -0.75 Å to +1 Å. For around 40% of the structures this distance is greater than 1.14 Å indicating no facial overlap between the molecules at all.

Fig. 6(e) depicts the frequency distribution of Cl-NII distance, the positive value of which indicates no edge overlap whereas a negative value indicates fractional facial overlap, the greater negative value means greater amount of ring crossing. From this figure one sees that for most of the structures the value of this parameter fall in the range 0.5 Å to 2.0 Å again indicating that the preferred stacking interaction for imidazole is an edge-to-edge one instead of a face to face one.

For the present crystal the above mentioned five parameters are (i) C-N distance 3.303 Å, (ii) the angle Cg1-Cl-NII is 107.41°; (iii) Perpendicular distance of the projection of Cg1 onto the ring plane of fragment-II (Cg1-M) is 1.638 Å (iv) The distance between Cl and NII is 0.998 Å; (v) The distance between Cg1 and Cg2 is 2.640 Å. Thus in consideration of the value of geometrical parameters as discussed in the previous section one can conclude that in the present crystal structure imidazole molecules interact through edge-to-edge supramolecular interaction.

The CSD database analysis strongly supports that the edge to edge supramolecular interaction among imidazole molecules should not be a crystal packing effect, but it may be assumed to be a true supramolecular interaction playing subtle role in directing the molecular self-assembly in many of the imidazole containing molecular crystals.

#### 3.1.5. Reduced Density Gradient and Non-covalent Interaction (NCI) study

Deeper insight regarding non-covalent interactions among molecular fragments is obtained from NCI isosurface plots [25]. In this plot, the reduced density gradient (Eq. (2)) is plotted against the product of electron density and the sign of the second Hessian eigenvalue [sign( $\lambda_2$ ) $\rho$ ]. The appearance of spikes in the negative region of this plot with small absolute magnitude is an indication of non-covalent interaction. Strength of this interaction is represented using colour codes. Red colour regions are having positive values and indicate repulsive steric interaction. Yellow to blue colour spikes in the negative region indicate stable attractive interactions such as hydrogen bonding. Van der Waals interaction is coded in green colour.

$$S = \frac{1}{2(3\pi^2)^{\frac{1}{3}}} \frac{|\nabla\rho|}{\rho^{4/3}} \quad (2)$$

Another variant of this plot is the NCI surface plot, in which the regions in 3D space are demarcated by isosurface values of the reduced electron density gradient. Regions of interaction are thus directly observed in the 3D space around the interacting molecules.

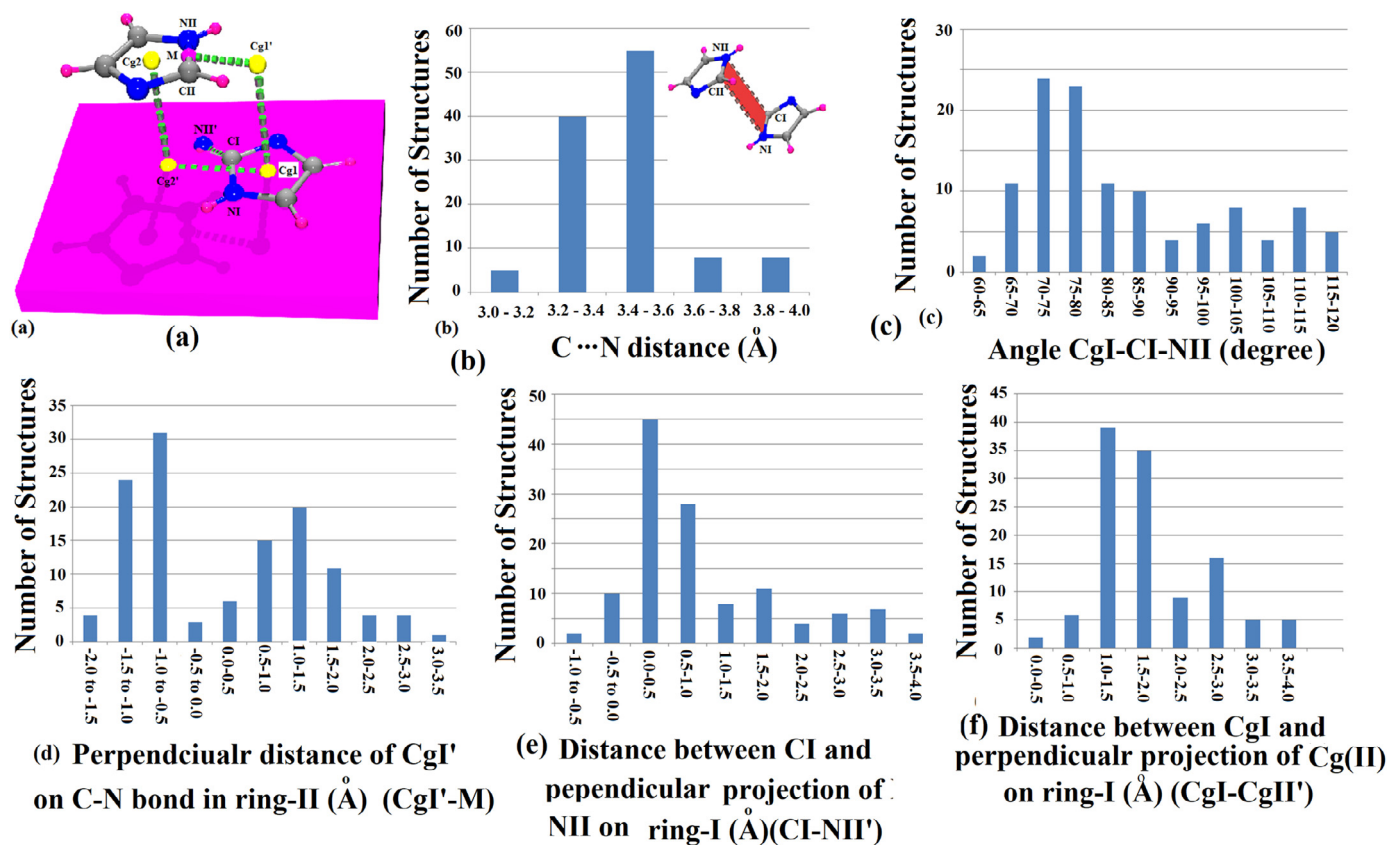


**Fig. 6.** Histogram plots of the edge to edge supramolecular interaction among molecules containing imidazole units in the CCDC database. (a) Geometry of interaction: Cg1 and Cg2 are ring centroids, whereas Cg1' and Cg2' are projected points of the centroids on the other ring plane, M is the middle of the CII-NII bond edge. Histogram plots of (b) Edge-to-edge CN distances (N1-ClI and Cl-NII) (c) Variation of the angle Cg1-Cl-NII (d) Variation of the perpendicular distance of Cg1' on the midpoint (M) of the ClI-NII bond edge (e) Distance between ClI and NII, the projection of NII on the ring I plane (f) Distance between Cg1 and Cg2; the projection of Cg2 on ring-I plane.

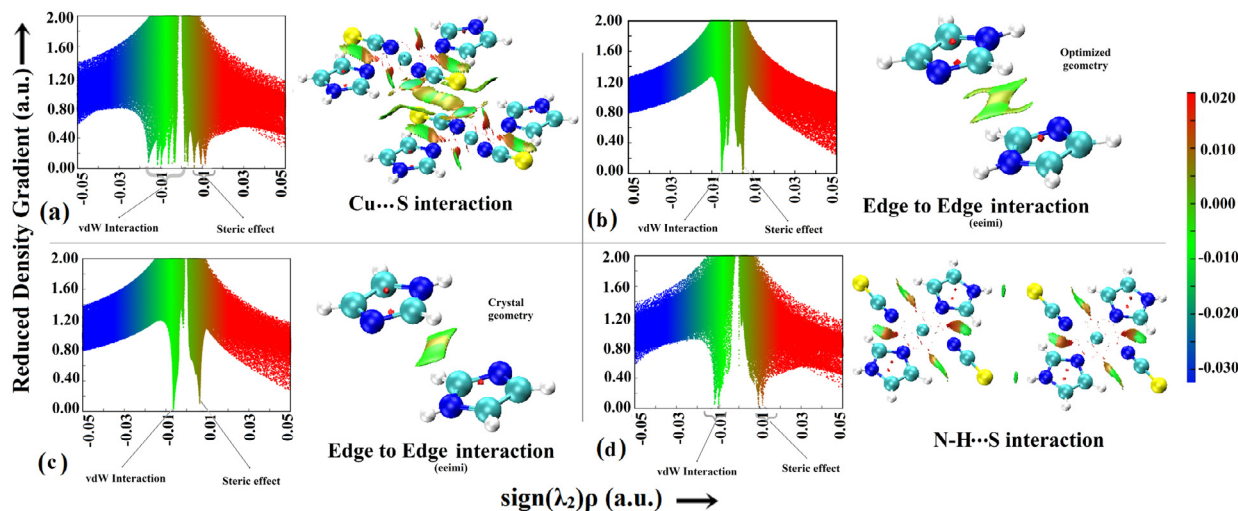


**Fig. 7.** RDG and NCI plots revealing non-covalent interactions in complex 1 have been presented in Fig. 7. RDG and NCI plots for two units of molecular complexes interacting through Cu...S, C-H...N, N-H...S, edge to edge supramolecular interaction of imidazole and van der Waals interaction has been depicted in Fig. 7a. Five distinct spikes in the negative values of  $\text{sign}(\lambda_2)\rho$  are present in the RDG

Similar colour codes for isosurface plots represent attractive to repulsive interactions.

RDG and NCI plots revealing non-covalent interactions in complex 1 have been presented in Fig. 7. RDG and NCI plots for two units of molecular complexes interacting through Cu...S, C-H...N, N-H...S, edge to edge supramolecular interaction of imidazole and van der Waals interaction has been depicted in Fig. 7a. Five distinct spikes in the negative values of  $\text{sign}(\lambda_2)\rho$  are present in the RDG

plot (left panel) which correspond to the above-mentioned interactions which are responsible for the packing of molecular complexes within the crystal. This analysis shows that the strongest interaction is Cu...S interaction ( $\text{sign}(\lambda_2)\rho = -0.016 \text{ a.u.}$ ), which is followed by N-H...S ( $\text{sign}(\lambda_2)\rho = -0.012 \text{ a.u.}$ ), C-H...N ( $\text{sign}(\lambda_2)\rho = -0.010 \text{ a.u.}$ ), edge to edge supramolecular interaction ( $\text{sign}(\lambda_2)\rho = -0.006 \text{ a.u.}$ ) and van der Waals interaction ( $\text{sign}(\lambda_2)\rho = -0.003 \text{ a.u.}$ ). The right-hand panel in Fig. 7a shows the NCI plot for the corre-

sponding interactions, where the isosurfaces of different area and colour representing the strength of interaction have been depicted. Strongest attractive interaction in the present system appears in green corresponding to the Cu...S interaction. Fig. 7b, Fig. 7c and Fig. 7d show these interactions computed for isolated motifs which shows that the spikes in isolation also appear nearly at the same values of  $\text{sign}(\lambda_2)\rho$ . Fig. 7b and Fig. 7c show the RDG and NCI plot for the edge to edge supramolecular interaction computed for only two edge to edge interacting imidazole molecules respectively in their crystal geometry and DFT optimized geometry. The spike corresponding to the edge to edge supramolecular interaction for both these cases appear nearly at the same value of  $\text{sign}(\lambda_2)\rho$  (-0.006 a.u.) indicating that the interaction strength for the computed geometry and the crystal geometry is nearly the same. NCI isosurfaces for this interaction has been shown in the right-hand panel of Fig. 7b and Fig. 7c which appear in light green. It is to be noted that the strength of this edge to edge supramolecular interaction in the present complex is nearly double of the van der Waals interaction but it is nearly half of the strength of the N-H...S interaction. The left panel of Fig. 7d shows the RDG plot for N-H...S and C-H...N interaction between two units in isolation. Corresponding NCI plot has been depicted on the right-hand panel of Fig. 7d.

### 3.1.6. Atoms in molecule analysis (AIM)

AIM analysis, introduced by Bader [26,27], explores the topology of electron density distribution in a given molecular system. The topological parameters such as bond critical points (BCPs), ring critical points (RCPs) and cage critical points (CCPs) are derived from this analysis which is indicative of the nature of intermolecular and intra-molecular interactions. These are the points where electron charge densities have maximum values. The numerical values of various topological parameters such as electron density ( $\rho$ ), Laplacian of electron density ( $\nabla^2\rho$ ), potential (V) and kinetic energy density (G) at BCPS have great importance as they are closely related to the nature and strength of the bond. The larger the value of ' $\rho$ ' at BCPS the stronger is the bond. The positive values of " $\nabla^2\rho$ " at bond critical points indicate that the interaction is of closed-shell or non-covalent nature and the electron charge density is depleted along the bond path. When the ratio  $\frac{|V|}{|G|}$  is less than unity at BCP then one can conclude that the interaction is non-covalent in nature.

We have carried out the AIM analysis to explore the relative importance of various weak non-covalent forces operating in the present crystal. Multiwfn program has been used for AIM analysis. The input to Multiwfn was prepared using GAUSSIAN-03 package at the DFT(B3lyp)6-311G(d,p) level of theory. The chosen motif for this analysis was determined from the knowledge of crystal packing analysis. As described previously, one can see that the complete set of intermolecular forces can be simulated by incorporating a set of four coordination complexes. This has been shown in Fig. 8a, where all weak intermolecular forces such as edge-to-edge supramolecular interaction of two imidazole moieties, C-H...S and N-H...S hydrogen bonding, as well as Cu...S interaction are present. Fig. 8a shows the computed BCPS (orange dots), RCPs (yellow dots) for this assembly. Bond paths have been denoted by green lines. For the clarity of understanding we have analyzed critical points for three sub-components of this composite system corresponding to edge-to-edge supramolecular interaction (Fig. 8b); C-H...S interaction (Fig. 8c) and Cu...S interaction (Fig. 8d).

The critical points for the edge-to-edge supramolecular interaction have computed for (i) the crystal geometry (Fig. 8b(i)) and (ii) the DFT optimized geometry (Fig. 8b(ii)) which is slightly different from the crystal geometry. Whereas there appears only a bond critical point for the crystal geometry (BCP7), the AIM analysis for the DFT optimized geometry gives rise to two bond critical points (BCP8 and BCP9) and a ring critical point (RCP10). A ring criti-

cal point is generated because of the generation of a supramolecular ring [C-N...C-N] involving two CN edges of two imidazole molecules. Table 2 shows that two BCPS (no 8 and 9) have nearly the same electron density ( $0.03 \text{ e}/\text{\AA}^3$ ) and the corresponding electron density at the ring critical point is  $0.03 \text{ e}/\text{\AA}^3$ . The  $\frac{|V|}{|G|}$  ratio for two BCPS 8 and 9 are the same (1.00). On the other hand, the  $\frac{|V|}{|G|}$  ratio for RCP 7 is 0.67. The  $\nabla^2\rho$  value for BCPS 8 and 9 are same ( $0.36 \text{ e}/\text{\AA}^5$ ) and for RCP 7 it is  $0.48 \text{ e}/\text{\AA}^5$  indicating the non-covalent nature of this interaction.

Fig. 8c shows the bond critical points (BCPs) for intermolecular N-H...S interaction and intramolecular CH...N interaction obtained through topological analysis of electron density the respective motifs. There are four BCPS - two each for NH...S interaction (1 and 3) and CH...N interaction (2 and 4). Calculated topological parameters such as electron density ( $\rho$ ), Laplacian of electron density ( $\nabla^2\rho$ ), the potential (V) and kinetic(G) energy density and their ratio ( $\frac{|V|}{|G|}$ ) have been listed in Table 2. At BCPS 1 and 3, the  $\rho$  and  $\nabla^2\rho$  values are  $0.08 \text{ e}/\text{\AA}^3$  and  $0.94 \text{ e}/\text{\AA}^5$  respectively. At BCPS 2 and 4, these values are respectively  $0.08 \text{ e}/\text{\AA}^3$  and  $1.19 \text{ e}/\text{\AA}^5$ . So the interaction is a closed shell in nature. The  $\rho$  value for N-H...S interaction is greater than that of C-H...N interaction indicating that NH...S is stronger interaction. The potential and kinetic energy ratios at BCPS are 0.80 and 0.71 for N-H...S (BCPs 1 and 3) and C-H...N (BCPs 2 and 4) interactions which comply with the non-covalent nature of these interactions.

Fig. 8d shows the bond critical points (BCPs) for intermolecular Cu...S interaction. The electron density at BCPS 5 and 6 have the same value ( $0.11 \text{ e}/\text{\AA}^3$ ). The  $\nabla^2\rho$  is  $1.05 \text{ e}/\text{\AA}^5$  and  $1.03 \text{ e}/\text{\AA}^5$  for 5 and 6 respectively, the ratios of  $\frac{|V|}{|G|}$  are 1.00 and 1.14 respectively. This indicates that this interaction is not of non-covalent and correlates with the Cu-S coordination interaction.

### 3.1.7. NICS study

Nucleus independent chemical shift analysis has become an important tool to characterize aromaticity and stability of chemical systems [28]. Generally, NICS has been utilized for covalent complexes. Positive values of NICS indicate anti-aromaticity and negative values aromaticity. As the edge-to-edge supramolecular motif is the stable supramolecular unit we have employed NICS to explore whether this possesses aromatic like character or not. The NICS(0) value has been depicted in Fig. 9. Iso-contour lines have been plotted which shows the nature of variation of NICS(0) value over the rectangular surface passing through the CN edges of two imidazole molecules that are involved in edge-to-edge supramolecular interaction. At the centre of the rectangle, the NICS(0) value is -7.2ppm which increases to -30ppm near the two CN edges. For benzene molecule, the NICS(0) value is -9ppm at the same level of theory [29].

Thus it can be concluded that the edge to edge supramolecular interaction motif of imidazole possesses benzene like aromatic character and is thus stable.

### 3.1.8. Hirshfeld Surface Analysis

Nowadays Hirshfeld surface analysis has become a popular tool to understand the relative importance of various atom..atom interactions in the packing of molecular units in a crystalline solid.

Fig. 10 shows Hirshfeld  $d_{\text{norm}}$  surfaces and 2D fingerprint plots for the four most prominent interactions governing crystal packing in the present crystal. Red spots in the respective plots correspond to the region of strong interactions, whereas blue regions on these surfaces correspond to areas which are more than van der Waals contacts. Fig. 10c shows red spots of varying intensity corresponding to these four interactions. Two deepest red spots in Fig. 10c corresponds to the most important N-H...S interaction for crystal packing. Corresponding 2D fingerprint plot has been shown

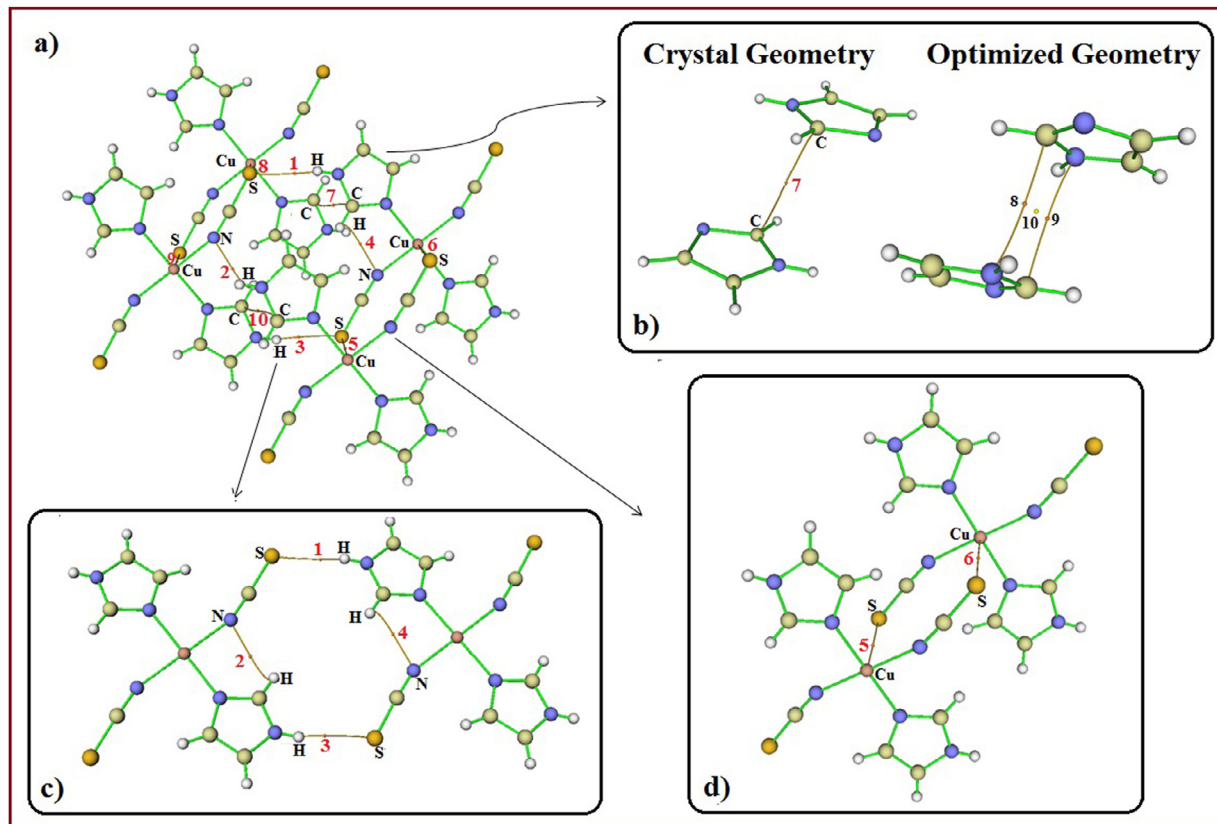


**Fig. 8.** BCPS are shown as the orange dots. (a) BCPS for all supramolecular interactions (b) (i) BCPS for imidazole edge to edge supramolecular interaction (Crystal geometry) (ii) DFT optimized geometry (c) BCPS for C-H...N and N-H...S interaction (d) BCPS for Cu-S interaction.

**Table 2**  
Electron density, Laplacian of electron density, Kinetic energy density and Potential energy density at respective bond critical points.

Between	CP	$\rho(r)$ Electron density $e/\text{\AA}^3$	$\nabla^2\rho$ Laplacian of electron density $e/\text{\AA}^5$	$V(r)$ Potential energy density $e/\text{\AA}^3$	$G(r)$ Lagrangian kinetic energy density $e/\text{\AA}^3$	$ V(r) /G(r)$	$G(r)/\rho(r)$
<b>NH...S and CH...N and interaction</b>							
S-H	1 & 3	0.08	0.94	-0.04	0.05	0.80	0.62
H-N	2 & 4	0.08	1.19	-0.05	0.07	0.71	0.87
<b>Cu-S interaction</b>							
Cu-S	5 & 8	0.11	1.05	-0.08	0.08	1.00	0.73
Cu-S	6 & 9	0.11	1.03	-0.08	0.07	1.14	0.64
<b>Imidazole edge to edge supramolecular interaction (eeimi) (Crystal geometry)</b>							
C-C	7	0.04	0.48	-0.02	0.03	0.67	0.75
<b>Imidazole edge to edge supramolecular interaction (eeimi) (Computed optimized geometry)</b>							
C-N	8 & 9	0.03	0.36	-0.02	0.02	1.00	0.67
	10	0.03	0.38	-0.02	0.02	1.00	0.67

in Fig. 10c'. There are two prominent spikes in this fingerprint plot for each of which the sum of  $d_i$  and  $d_e$  is  $\sim 2.4\text{\AA}$  which corresponds to the bond length of N-H...S interactions. The contribution of this interaction with respect to the total is 21.9%.

A pair of relatively lighter red spots in Fig. 10c (shown within the elliptical ring) corresponds to Cu...S interactions. The central spot in this pair correspond to Cu of one unit and outer spot correspond to S of a complementary unit. This has been shown separately in Fig. 10d and the corresponding fingerprint plot has been shown in Fig. 10d'. This pair of red spots correspond to the coordination bond between Cu and S. This leads to a coordination polymeric nature of the complex. Two prominent spikes in this fingerprint plot having the sum of  $d_i$  and  $d_e$  as  $\sim 3.06\text{\AA}$  correspond to this Cu...S interaction which is the coordination interaction between Cu

and S. The contribution of this interaction within the total fingerprint area is 5.1%.

A set of two other relatively faint red spots can be seen in Fig. 10c (marked with rings). One of these is encircled within a bigger ring which corresponds to C...C (imidazole edge to edge supramolecular interaction and this has been depicted in Fig. 10b in a different orientation. The lightest red spot encircled within the smaller ring in Fig. 10c corresponds to S...C interaction and this has been separately shown in Fig. 10a. Corresponding fingerprint plots respectively are shown in Fig. 10a' and Fig. 10b'. The C...C interaction has a broad fingerprint spot (Fig. 10b') which can be assigned to the edge-to-edge supramolecular interaction between the imidazole molecules. The sum of  $d_i$  and  $d_e$  for this is  $3.30\text{\AA}$ . Percentage contribution of this interaction is 1.7%. Fig. 10a' shows the fingerprint plot for the S...C interaction, two spikes are corre-

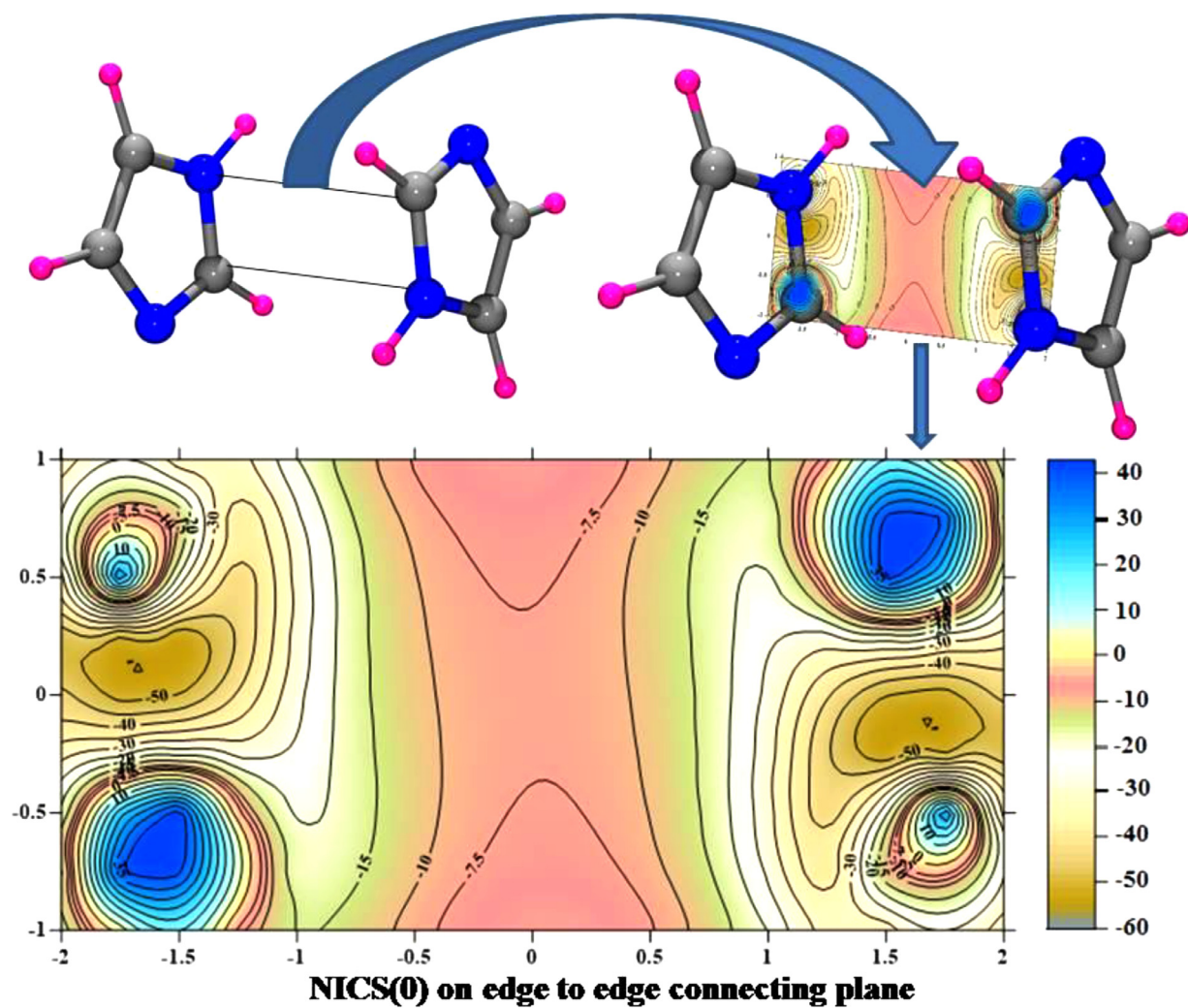


**Fig. 9.** NICS(0) surface plot for the plane the edges of the two imidazole molecule.

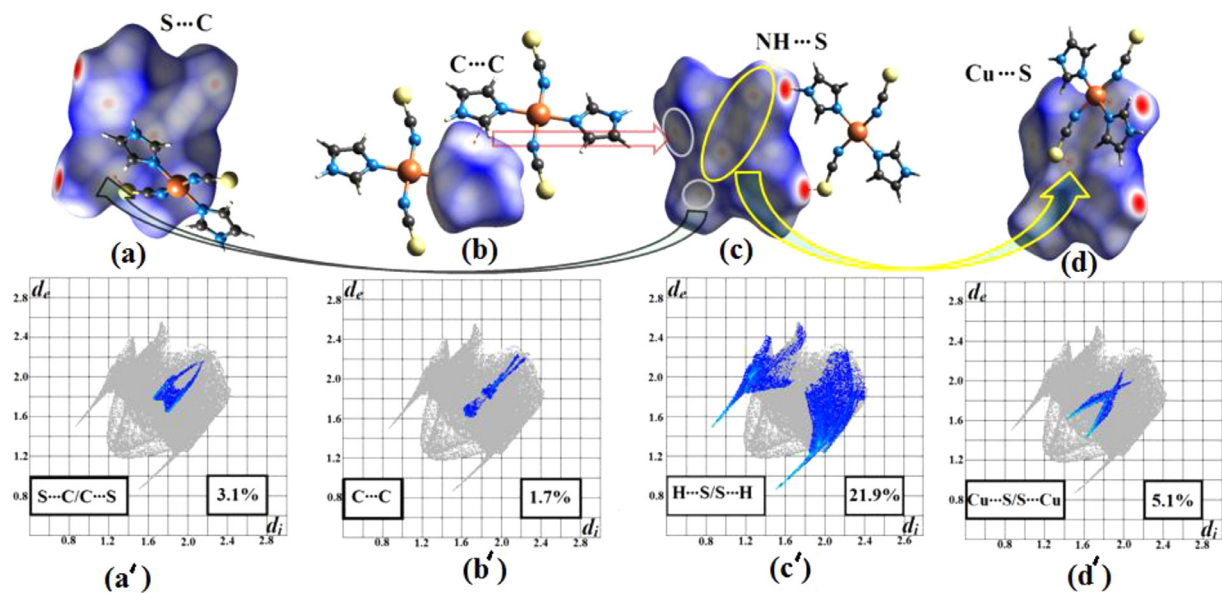


**Fig. 10.** 3D Hirshfeld surface and corresponding 2D fingerprint plots.

sponding to this interaction, but the spikes are not as pointed as that for N-H...S or Cu...S interactions. The sum of  $d_i$  and  $d_e$  for this interaction is ~3.5 Å. The percentage contribution of this interaction in crystal packing is 3.1%.

The fingerprint plots for all interactions have been depicted in Fig. S1(a). The breakup of this plot into individual plots has been shown in Fig. S1(b), (c), (d), (e) and (f).

A closer look at the hirshfeld surface analysis as well as fingerprint plots reveals that crystal packing is a holistic effect of strong as well as weak interactions. Though N-H...S or Cu...S interactions play dominant role in crystal packing, the role played by other weaker forces such as eeimi interaction and H...H interaction mostly representing van der Walls contact contribute their share in the crystal packing.

#### 4. Discussion

Weak intermolecular interactions are of fundamental importance in molecular self-assembly and crystal engineering. An edge to edge imidazole interaction so far unreported has been explored experimentally through crystal structure analysis along with CCDC database exploration as well as through theoretical studies. In this novel interaction there is nearly no facial overlap; two imidazole molecules only interact through their CN edges. A horizontal shift of one of the interacting molecules along the perpendicular direction to the CN edges shows a prominent deep in the interaction potential which can be assigned to this edge to edge interaction. This kind of deep in interaction potential has been reported by Prof. S. Zaric [30,31] who has extensively studied the chelate ring cycle stacking interaction of square planar metal complexes which is also a relatively newly reported interaction. The interaction energy of this kind of chelate chelate interaction has been reported to be -6.51 kcal/mole to -9.70 kcal/mole.[32] The edge to edge imidazole interaction energy being reported here is even weaker (-2.59 kcal/mole) in strength. The strength of the NH...S hydrogen bond between the imidazole unit and the thiocyanate unit was estimated at the same level of theory as that of edge to edge imidazole interaction (eeimi). The BSSE corrected binding energy for this interaction was found to be -17.02 kcal/mole which is nearly six times stronger than the eeimi interaction. It is to be noted that the self-assembly in the crystal by the strong NH...S bond and weak eeimi interaction is in mutually orthogonal direction which makes them compatible with each other and both are simultaneously present in the crystal. eeimi interaction in this fashion not only operates in the present crystal but also it plays similar definitive role in molecular self-assembly in many of the crystal structures already present in the CCDC database. This has been manually checked for individual crystal structures retrieved from the CCDC database.

#### 5. Conclusion

Self-assembly through weak intermolecular forces is fundamental to almost all biochemical processes. Efforts to understand the various features of the self-assembly process are currently being pursued vigorously in many areas of science and technology to gain better control over the self-assembly process. One important area where this knowledge is going to be important is the design and operation of functional nano-scale devices. Crystalline materials grow through the natural self-assembly of molecules, counterions and metal ions. Each of these components encodes how intermolecular and ionic forces will be expressed in a given system which not only depends on the nature of the components themselves but also on the physicochemical conditions at which these components are uniting. The self-assembled system of just three simple components, imidazole, thiocyanate ion

and Cu(II) ion which is the subject of the present study, is expected to be very simple. Yet, the mutual role of intermolecular forces is quite subtle. NH...S and CH...S hydrogen bonding interaction, imidazole-imidazole edge to edge supramolecular interaction and the Cu...S coordinative interaction are responsible for self-assembly here. The most interesting observation is that of the edge to edge supramolecular interaction among imidazole units. This study shows that edge-to-edge supramolecular interaction is a characteristic of imidazole moiety and this interaction has played a role in crystal packing in the present crystal structure. CSD database analysis also shows that edge-to-edge supramolecular interaction is a statistically significant one for many crystals which contain imidazole as one of the components which self-assemble. Interaction strength of this edge-to-edge interaction of imidazole molecules is in the range of very weak intermolecular forces, yet this interaction remains significant in the presence of presumably stronger Cu...S coordinative forces and N-H...S hydrogen bonding forces. Mutual competition of these forces has made Cu...S distance relatively large compared to that found in other coordination complexes. Thus the present crystal structure is a typical example where weak force competes with coordinative force. In summary, in-depth analysis of weak forces in the present crystal structure has led us to recognize an edge to edge supramolecular interaction among imidazole molecules which remained unnoticed so far. The mutual coexistence of several of intermolecular forces having a hierarchy of weak, weaker and strong nature show that cooperativity of weaker forces can lead to the weakening of stronger forces as is evident by longer Cu...S coordination bond in the present crystal.

#### Credit author statements

Sirajuddin Sarkar Methodology, Data curation. Sourav Ranjan Ghosh Software, Computation. Paula Brandão Data Curation, Atish Dipankar Jana Conceptualization, Writing- Reviewing and Editing.

#### Declaration of Competing Interest

The authors declare that they have no known competing financial interests or personal relationships that could have appeared to influence the work reported in this paper.

#### Acknowledgement

Atish Dipankar Jana acknowledges the financial support from the department of Science, Technology and Biotechnology, Government of West Bengal, India through the project memo no 250 (Sanc.)/ST/P/S&T/16G-47/2017 Date: 25/03/2018.

#### References

- [1] G.R. Desiraju, C-H O and other weak hydrogen bonds. From crystal engineering to virtual screening, *J. Chem. Soc., Chem. Commun* (2005) 2995–3001, doi:[10.1039/b504372g](https://doi.org/10.1039/b504372g).
- [2] G. Cavallo, P. Metrangolo, R. Milani, T. Pilati, A. Priimagi, G. Resnati, G. Terraneo, The Halogen Bond, *Chemical Reviews* 116 (4) (2016) 2478–2601, doi:[10.1021/acs.chemrev.5b00484](https://doi.org/10.1021/acs.chemrev.5b00484).
- [3] M. Ponce-Vargas, A. Muñoz-Castro, Heavy Element Metallocycles: Insights into the Nature of Host–Guest Interactions Involving Dihalide Mercuramacrocyclic Complexes, *J. Phys. Chem. C* 118 (2014) 28244–28251, doi:[10.1021/jp5092625](https://doi.org/10.1021/jp5092625).
- [4] D. Blasco, J.M. López-de-Luzuriaga, M. Monge, M.E. Olmos, D. Pascual, M. Rodríguez-Castillo, Cooperative Au(I) Au(I) Interactions and Hydrogen Bonding as: Origin of a Luminescent Adeninate Hydrogel Formed by Ultrathin Molecular Nanowires, *Inorg. Chem.* 57 (2018) 3805–3817, doi:[10.1021/acs.inorgchem.7b03131](https://doi.org/10.1021/acs.inorgchem.7b03131).
- [5] C. Wang, D. Liu, W. Lin, Metal-organic frameworks as a tunable platform for designing functional molecular materials, *J. Am. Chem. Soc.* 135 (2013) 13222–13234, doi:[10.1021/ja308229p](https://doi.org/10.1021/ja308229p).
- [6] B.A. Grzybowski, K. Fitzner, J. Paczesny, S. Granick, From dynamic self-assembly to networked chemical systems, *Chem. Soc. Rev.* 46 (2017) 5647–5678, doi:[10.1039/c7cs00089h](https://doi.org/10.1039/c7cs00089h).

- [7] N. Mittal, I. Paul, S. Pramanik, M. Schmittel, Remote control of the reversible assembly/disassembly of supramolecular aggregates, *Supramolecular Chemistry* (2020) 10.1080/10610278.2020.1711907.
- [8] H. Y. Lee, S. H. R. Shin, A. M. Drews, A. M. Chirisan, S. A. Lewis and K. J. M. Bishop, Self-Assembly of Nanoparticle Amphiphiles with Adaptive Surface Chemistry *ACS Nano*, 8 (2014) 9979–9987 doi: 10.1021/nn504734v.
- [9] K. Bhattacharyya, A. Surendran, C. Chowdhury, A. Datta, Steric and electric field driven distortions in aromatic molecules: spontaneous and non-spontaneous symmetry breaking, *Phys. Chem. Chem. Phys* 18 (2016) 31160–31167, doi: 10.1039/c6cp05237a.
- [10] C. Lefebvre, G. Rubez, H. Khatabil, J.C. Boisson, J. Contreras-García, E. Hénon, Accurately extracting the signature of intermolecular interactions present in the NCI plot of the reduced density gradient: Versus electron density, *Phys. Chem. Chem. Phys* 19 (2017) 17928–17936, doi: 10.1039/c7cp02110k.
- [11] K. Gholivand, K. Farshadfar, S.M. Roe, M. Hosseini, A. Gholami, Investigation of structure-directing interactions within copper(i) thiocyanate complexes through X-ray analyses and non-covalent interaction (NCI) theoretical approach, *CrystEngComm* 18 (2016) 7104–7115, doi: 10.1039/c6ce01339b.
- [12] P.R. Varadwaj, A. Varadwaj, B.Y. Jin, Hexahalogenated and their mixed benzene derivatives as prototypes for the understanding of halogen halogen intramolecular interactions: New insights from combined DFT, QTAIM-, and RDG-based NCI analyses, *J. Comput. Chem.* 36 (2015) 2328–2343, doi: 10.1002/jcc.24211.
- [13] C. Foroutan-Nejad, S. Shahbazian, R. Marek, Toward a consistent interpretation of the QTAIM: Tortuous link between chemical bonds, interactions, and bond/line paths, *Chem. - A Eur. J* 20 (2014) 10140–10152, doi: 10.1002/chem.201402177.
- [14] Z. Chen, C.S. Wannere, C. Corminboeuf, R. Puchta, P. von Ragué Schleyer, Nucleus-independent chemical shifts (NICS) as an aromaticity criterion, *Chem. Rev* 105 (2005) 3842–3888, doi: 10.1021/cr030088.
- [15] S. Martín-Santamaría, H.S. Rzepa, Double aromaticity and anti-aromaticity in small carbon rings, *Chem. Commun.* (2000) 1503–1504, doi: 10.1039/b00292j.
- [16] G. Desiraju, *Perspective in supramolecular chemistry- Crystal as a supramolecular entity* Ed. John Wiley & sons, 1996.
- [17] M.A. Spackman, D. Jayatilaka, Hirshfeld surface analysis, *CrystEngComm* 11 (2009) 19–32, doi: 10.1039/B818330A.
- [18] G.M. Sheldrick, *SHELXT – Integrated space group and crystal structure determination*, *Acta Cryst A* 71 (2015) 3–8.
- [19] G.W. M.J. Frisch, H.B. Trucks, G.E. Schlegel, M.A. Scuseria, J.R. Robb, J.J.A. Cheeseman, T. Montgomery, K.N. Kudin, J.C. Vreven, J.M. Burant, S.S. Millam, J. Iyengar, V. Tomasi, B. Barone, M. Mennucci, G. Cossi, N. Scalmani, G.A. Rega, H. Petersson, M. Nakatsuji, M. Hada, K. Ehara, R. Toyota, J. Fukuda, M. Hasegawa, T. Ishida, Y. Nakajima, O. Honda, H. Kitao, M. Nakai, X.Li, J.E. Klene, H.P. Knox, J.B. Hratchian, C. Cross, J. Adamo, R. Jaramillo, R.E. Comperts, O. Stratmann, A.J. Yazyev, R. Austin, C. Cammi, J.W. Pomelli, P.Y. Ochterski, K. Ayala, G.A. Morokuma, P. Voth, J.J. Salvador, V.G. Dannenberg, S. Zakrzewski, A.D. Dapprich, M.C. Daniels, O. Strain, D.K. Farkas, A.D. Malick, K. Rabuck, J.B. Raghavachari, J.V. Foresman, Q. Ortiz, A.G. Cui, S. Baboul, J. Clifford, B.B. Cioslowski, G. Stefanov, A. Liu, P. Liashenko, I. Piskorz, R.L. Komaromi, D.J. Martin, T. Fox, M.A. Keith, C.Y. Al-Laham, A. Peng, M. Nanayakkara, P.M.W. Challacombe, B. Gill, W. Johnson, M.W. Chen, C. Wong, J.A. Gonzalez, Pople, Gaussian 03, revision C.02, Gaussian, Wallingford CT, 2004 Inc.
- [20] GAMESS, 2016-Pgi-linux-mkl, Multiwfns: A multifunctional wavefunction analyzer, *J. Comput. Chem.* 33 (2012) 580–592, doi: 10.1002/jcc.22885.
- [21] S.K. Wolff, D.J. Grimwood, J.J. McKinnon, M.J. Turner, D. Jayatilaka, M.A. Spackman, University of Western Australia, 2012.
- [22] M.D. Curtis, J. Cao, J.W. Kampf, Solid-State Packing of Conjugated Oligomers: From  $\pi$ -Stacks to the Herringbone Structure, *J. Am. Chem. Soc.* 126 (2004) 4318–4328, doi: 10.1021/ja0397916.
- [23] P. Hobza, H.L. Selzle, E.W. Schlag, Potential energy surface for the benzene dimer. Results of ab initio CCSD(T) calculations show two nearly isoenergetic structures: T-shaped and parallel-displaced, *J. Phys. Chem.* 100 (1996) 18790–18794.
- [24] A. Otero-De-La-Roza, E.R. Johnson, J. Contreras-García, Revealing non-covalent interactions in solids: NCI plots revisited, *Phys. Chem. Chem. Phys* 14 (2012) 12165–12172, doi: 10.1039/c2cp41395g.
- [25] R.F.W. Bader, *Atoms in molecules - A quantum theory*, Clarendon Press, Oxford, 1994.
- [26] F. Weinhold, Natural Bond Critical Point analysis: quantitative relationships between natural bond orbital-based and QTAIM-based topological descriptors of chemical bonding, *J. Comput. Chem.* 30 (2012) 2440–2449, doi: 10.1002/jcc.23057.
- [27] C. Foroutan-Nejad, S. Shahbazian, P. Rashidi-Ranjbar, The electron density vs. NICS scan: A new approach to assess aromaticity in molecules with different ring sizes, *Phys. Chem. Chem. Phys.* 12 (2010) 12630–12637, doi: 10.1039/c004254d.
- [28] Z. Chen, C.S. Wannere, C. Corminboeuf, R. Puchta, P.V.R. Schleyer, Nucleus-independent chemical shifts (NICS) as an aromaticity criterion *Chem. Rev* 105 (2005) 3842–3888.
- [29] D. P. Malenova, G. V. Janjic ; M. B. Hallc, Snežana D. Zaric, Noncovalent bonding: Stacking interactions of chelate rings of transitionmetal complexes *Coordination Chemistry Reviews* 345 (2017) 318–341.
- [30] Z.D. Tomic , D. Sredojevic , and Snež , D. Zaric , Stacking Interactions between Chelate and Phenyl Rings in Square-PlanarTransition Metal Complexes, *Cryst. Growth. Des* 6 (1) (2006) 29–31.
- [31] D.P. Malenov, S.D. Zarić, Chelated metal ion modulates the strength and geometry of stacking interactions: energies and potential energy surfaces for chelate-chelate stacking, *Physical Chemistry Chemical Physics* 20 (2018) 14053–14060.